SSCL-374

Superconducting Super Collider Laboratory

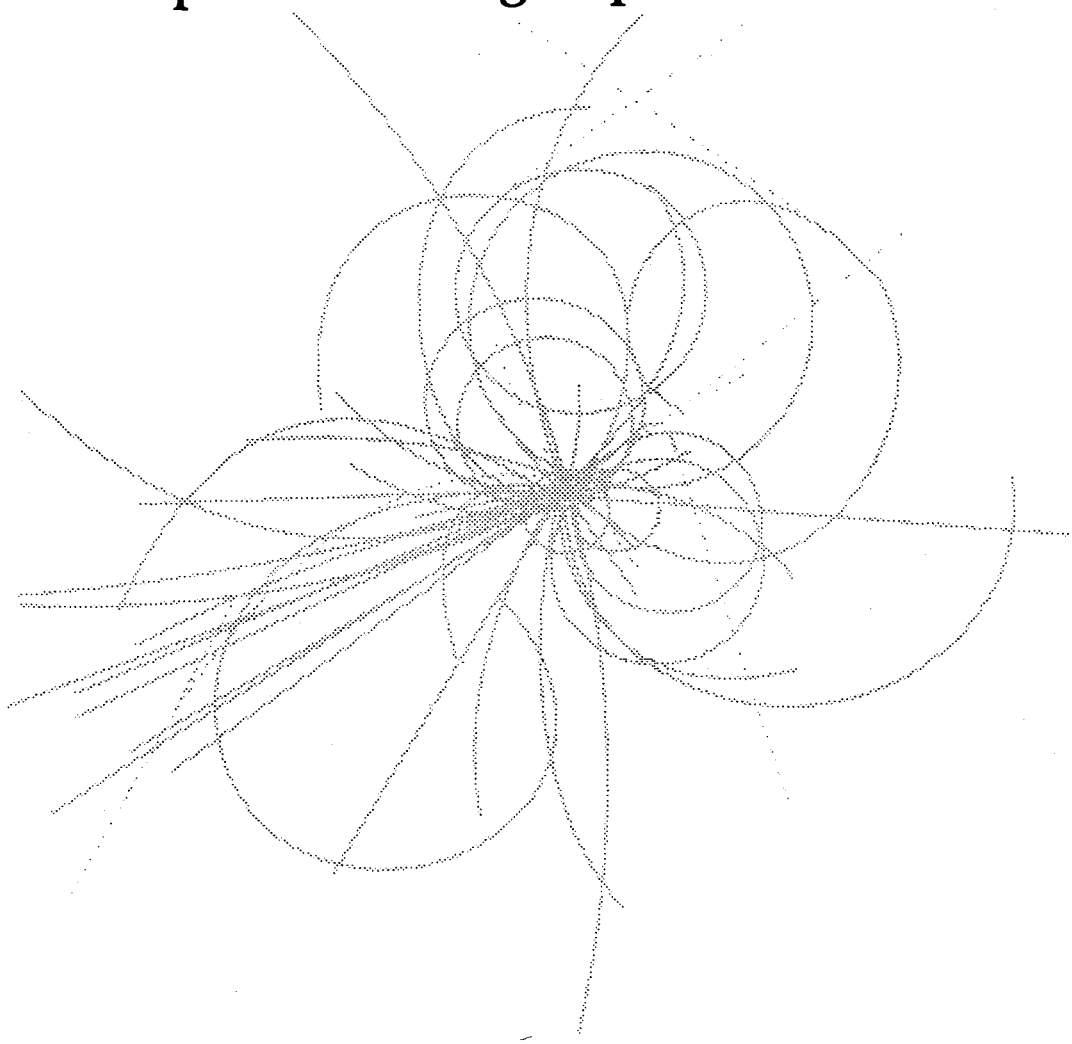

Design and A.C. Loss Considerations for the 60 mm Dipole Magnet in the High Energy Booster

G. Snitchler, R. Jayakumar, V. Kovachev, and D. Orrell

April 1991

SSCL-374

DESIGN AND A.C. LOSS CONSIDERATIONS FOR THE 60 mm DIPOLE MAGNET IN THE HIGH ENERGY BOOSTER*

G. Snitchler, R. Jayakumar, V. Kovachev, and D. Orrell

Magnet Systems Division
Superconducting Super Collider Laboratory†
2550 Beckleymeade Avenue
Dallas, TX 75237

April 1991

* Presented at the Third International Industrial Symposium on the Super Collider, Atlanta, Georgia, March 13-15, 1991.

† Operated by the Universities Research Association, Inc., for the U.S. Department of Energy under Contract No. DE-AC02-89ER40486.

DESIGN AND A.C. LOSS CONSIDERATIONS FOR THE 60 MM DIPOLE MAGNET IN THE HIGH ENERGY BOOSTER

G. Snitchler, R. Jayakumar, V. Kovachev, and D. Orrell

Magnet Systems Division
Superconducting Super Collider Laboratory*
2550 Beckleymeade Ave., Dallas, TX 75237

ABSTRACT

The baseline design for the SSC High Energy Booster (HEB) has dipole bending magnets with a 50 mm aperture. A recent dynamic aperture study for the High Energy Booster (HEB) suggests that an increased aperture dipole magnet (DM) is desirable. Two cost neutral options for a 60 mm aperture HEBDM design are investigated. Field transfer function, field harmonics, and relative cost impact for these designs are presented. An analysis of the cryogenic heat load due to A.C. losses generated in the HEB ramp cycle are also reported. Included in this analysis are losses from superconductor hysteresis, yoke hysteresis, strand eddy currents, and cable eddy currents. The A.C. loss impact of 2.5 μm vs. 6 μm filament conductor will be presented. Superconducting proximity effect is also considered for 2.5 μm filament conductors.

INTRODUCTION

As a result of a recently completed dynamic aperture study for the High Energy Booster (HEB), it has become apparent that investigation of an increased aperture dipole magnet (DM) is desirable.[1] The two cost neutral options for the HEB involving a 60 mm aperture HEBDM are: 1) a decreased field magnet installed into the SCDR[2] HEB circumference ring, and 2) a SCDR specified field magnet installed into a decreased circumference ring.

The high energy booster (HEB) dipole magnet (DM) has a different set of operating conditions compared to the collider dipole magnet (CDM). The current specifications for HEBDM operation involves eight bipolar ramp cycles which provides a continuous heat load due to A.C. losses during injection to the collider ring.

In the Site Specific Conceptual Design (SCDR), the HEBDM was specified to have the same design as the CDM. Studies indicate that a 50 mm aperture HEBDM is too small for cryogenic and dynamic aperture needs. A larger aperture would improve the removal of heat with more annular space for the required beam tube size and also provide higher field quality to increase the dynamic aperture. This report addresses options for a 60 mm aperture HEBDM. Section (1) covers design alternatives and parameters for a 60 mm aperture magnet. In section (2), A.C. losses are discussed and estimated. The impact of A.C. losses on HEB operation will be discussed in a another paper.[3]

* Operated by Universities Research Association, Inc., for the U.S. Department of Energy under Contract No. DE-AC02-89ER40486.

(1) DESIGN CONFIGURATIONS OF HEB DIPOLE

Several 60 mm aperture HEBDM designs were developed to perform cost estimates, lattice considerations, and for A.C. loss studies. While this report is not intended to be a formal presentation of an HEBDM design, a more detailed description of a 60 mm design will be published in a separate report.[4] The T5 60 mm design presented in this report represents a reasonable magnet for a 1.8 TeV collider operating at 5.8 T. A second design, called T11, represents a design with the same central field as the 50 mm design with perhaps an upper limit for the superconductor volume in a two coil cosine theta magnet design with required characteristics.

Table 1.1 CHOICE OF THE DESIGN FOR HEB DIPOLE

	50 mm (CDM design)	60 mm (T5 - HEB)	Comments
conductor:			
inner	30 strands	28 strands	8% less
inner	19 turns	25 turns	
outer	36 strands	32 strands	
outer	26 turns	23 turns	
sc volume/15m (m^3)	0.0136	0.0138	
collar+yoke vol (m^3)	1.25	1.2	
oper. field (T)	6.38	5.8	
oper. cur (a)	6250	5950	
oper. cur. den. (a/mm^2)	1015	1036	inner
saturation %	2.35	1.75	
peak field (T)	6.7	6.2	
quench current (a)	7270	7310	
quench peak field (T)	7.6	7.4	
que cur den (a/mm^2) (inner)	1181	1272	11% higher
quench field (T)	7.27	6.96	4.4% higher
MARGIN			
quench field %	13.9	20	
quench current %	16.3	22.3	6% higher
temp. margin (K)	0.75	1.1	

A mature version of the T5 design would be an adequate HEBDM design and will serve as the basis of comparison to contrast with the CDM design. In table (1.1), T5 and CDM design parameters are presented. The T5 design has two wedges on the inner layer and no wedges on the outer layer. The CDM has three wedges in the inner coil and one wedge in the outer coil. The T5 inner and outer cables have strand sizes matching that of the CDM. The coils have 28 and 32 strands for the inner and outer cables respectively, as opposed to 30 and 36 strands for the CDM. The keystone angle of the outer layer has been increased to 1.57 degrees to allow full radial positioning of the cables. This is not expected to have any significant effect on cable degradation.

The T5 design has 48 turns: 25 inner turns and 23 outer turns. In contrast, the CDM design has 19 turns on the inner layer and 26 on the outer. The collider dipole requires more wedges because of the smaller bore tube relative to cable keystone. T5 and the CDM both use the same volume of superconductor to meet the cost neutrality requirement. The field from the T5 design can be increased by widening the cable, the limit being set by the maximum size cable attainable. A large number of models were tested to establish a plot of field vs superconductor volume. A central field of 6.6 T, the same as the collider dipole, cannot be reached with adequate margin without using an excessively wide cable (at least 40 strands).

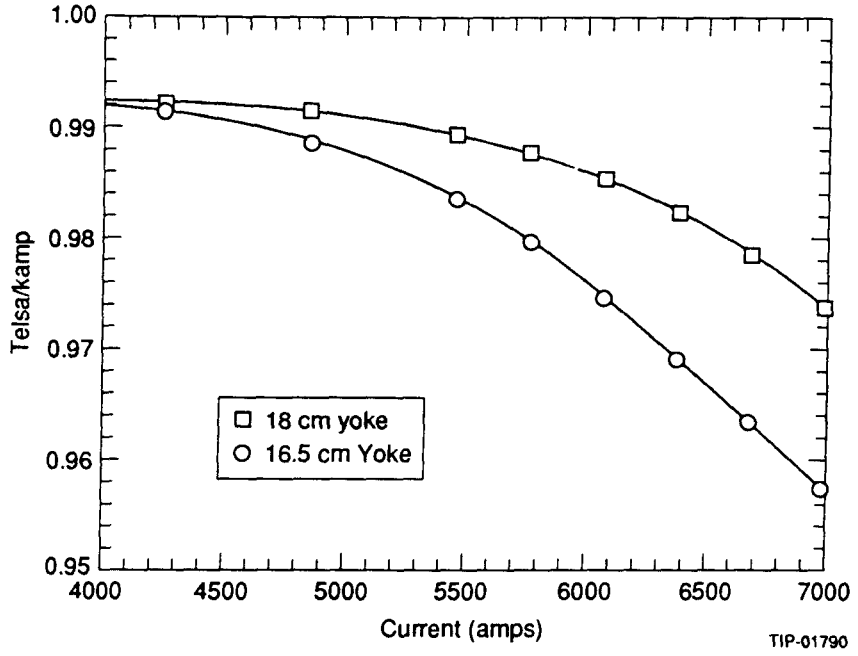

Figure 1.1 - Transfer Function of T5 HEBDM

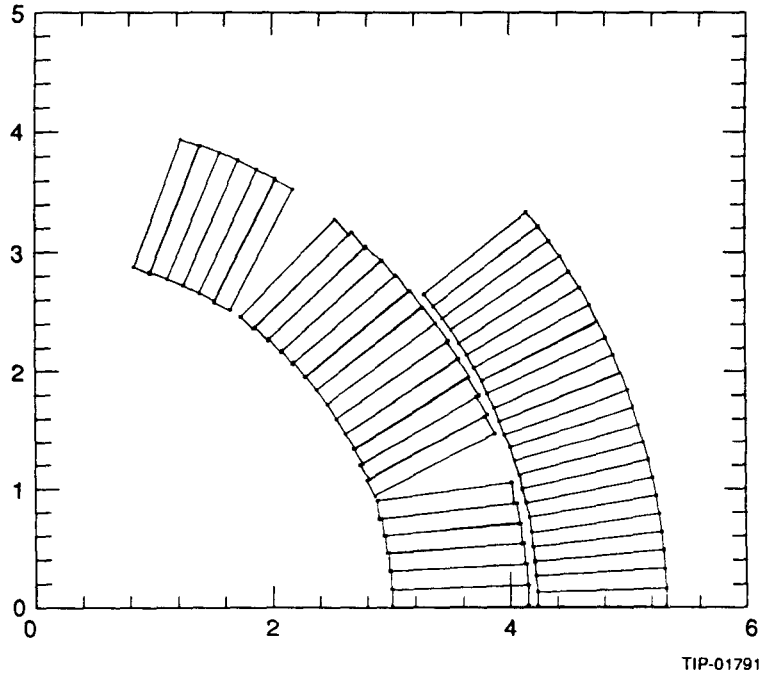

Figure 1.2 - Coil configuration of T5 HEBDM

The T5 magnet has been modelled using the finite element code PE2D to establish its behaviour with a saturable yoke. An outer radius to the iron yoke with 16.5 cm radius gives 1.75% nonlinearity in the transfer function at 5.8 Tesla as seen in figure (1.1). This can be decreased to 0.6% with an outer yoke radius of 18 cm. The nonlinearity at 6.4 Tesla with the 16.5 cm radius yoke gives a saturation of nearly 4% and the 18 cm yoke has a saturation of 2.2%. This will be a significant disadvantage in upgrading the HEBDM for 2 TeV operation.

The yokes were modelled without any features such as bus bars or keys which would increase saturation slightly. Depending upon the availability of cryostat space, a yoke radius larger than 16.5 cm may be explored to reduce the saturation. The smaller yoke also shows considerable change in b2 during the ramp which may require insertion of a special key for correction purposes. The margin in field expected for this magnet has been calculated taking into account the nonlinear ramp, and was found to be 20% above 5.8 T for the 16.5 cm outer yoke radius.

The T11 60 mm HEBDM design represents the second option of a higher field magnet. This design is a two layer magnet with 51 turns: 6 turns at the midplane, a wedge, 13 turns, a wedge, and 6 turns at the pole in the inner coil and one conductor block in the outer coil of 26 turns. The T11 design achieves 20% margin in field only at 6.25T with a nonlinearity of 2.12%. This may be compared with the 50 mm CDM design, which obtains 20% margin only at about 6.1 T. The T11 60 mm aperture design is not considered to be an efficient design for the HEB but is used here as a demonstration of the impact of more superconductor on A.C. losses.

(2) A.C. LOSSES ANALYSIS

The major technical design consideration for the HEBDM is the heat loss due to ramping cycles or usually referred to as A.C. losses. The major sources of A.C. loss are magnetization hysteresis in the yoke and the superconductor, and eddy current losses in the cable volume. Estimates for these losses are presented in the following sections. A combined set of losses for several magnet designs are presented in section (2.6). It is once again emphasized that the 60 mm designs presented are primarily for A.C. loss studies and do not constitute mature designs.

(2.1) Hysteresis loss in Superconductor

Irreversible magnetization occurs due to structural irregularities in the superconducting material acting as pinning centers for fluxoids. These pinning sites restrain magnetic flux motion when the magnetic field is changed. On the other hand, the viscous motion of the flux lines due to Lorentz forces in the current carrying region leads to a resistive state and non-zero electric field within the superconductor.

Hysteresis losses of a multifilament conductor exposed to a changing magnetic field depend on the superconducting critical current density $J_c(B,T)$, the diameter of the filaments, d_f, the twist pitch length, L, the range of magnetic induction change from 0 and B_m and the orientation of the magnetic field regarding the conductor axis. These losses are related to a cycle of magnetic field change and are not dB/dt dependent.

During the HEBDM operations the multifilament conductor is exposed to various values of magnetic field B depending on its position in the inner or outer coil of the magnet configuration. To determine precisely the local or average value of B for a particular conductor the magnetic induction distribution for the entire coil volume must be known. This information is also required for determination of the local or average value of critical current density in a particular region of the magnet coils.

The standard bulk magnetization approximation for cylindrical geometry filaments is expressed as

$$M = \frac{2}{3\pi}\mu_o J_c d_f (1 - \frac{J}{J_c}) \tag{2.1.1}$$

where d_f is the diameter of the filament, J the current density during the ramp cycle, and J_c is the critical current density at a given filament's field and operating temperature. A bulk

model for magnetization is justified because the magnetic field fully penetrates the filaments at $B > \mu_o J_c(B) d_f/2$. The energy dissipated during a ramp from zero to B_m can be expressed as

$$Q_h^s = \frac{1}{\mu_o} \int_0^{B_m} M dB \tag{2.1.2}$$

assuming that B_m, is a local maximum. Two methods have been employed to compute the J_c in the conductor and evaluate the integral in equation (2.1.2). The first technique involves an analytic formula for the field profile during the ramp cycle and a second technique numerically computes B in the coil volume in an infinite-iron approximation. Also, the more accurate numerical simulations use a J_c surface derived from experimental data.[5]

An analytic approximation requires a simple approximation for the critical current density. J_c can be approximated using the Kim-Anderson model[6] as

$$J_c = \frac{J_{co} B_o}{B + B_o} = \frac{2 J_c(B_o) B_o}{B + B_o} \tag{2.1.3}$$

where J_{co} and B_o represent the characteristics of the material and $J_c(B_o) = J_{co}/2$. By substituting equations (2.1.3) and (2.1.1) into equation (2.1.2) and integrating, we obtain

$$Q_h^s = \frac{8}{3\pi} d_f J_c(B_o) B_o ln(\frac{B_m + B_o}{B_o}). \tag{2.1.4}$$

The local maximum field achieved during a ramp cycle varies within the coil. An approximate estimate of this effect can be obtained by assuming a linear field distribution from a B_1 to B_2. The resulting average heat generation is

$$\begin{aligned} \langle Q_h^s \rangle &= \frac{8}{3\pi} d_f \frac{J_c(B_o) B_o}{B_2 - B_1} \int_{B_1}^{B_2} ln \frac{B_m + B_o}{B_o} dB_m \\ &= \frac{8}{3\pi} d_f \frac{J_c(B_o) B_o^2}{B_2 - B_1} [\frac{B_2 + B_o}{B_o} (ln(\frac{B_2 + B_o}{B_o}) - 1) \\ &- \frac{B_1 + B_o}{B_o} (ln(\frac{B_1 + B_o}{B_o}) - 1)]. \end{aligned} \tag{2.1.5}$$

The average power production is

$$\langle W_h^s \rangle = \langle Q_h^s \rangle \frac{\lambda V}{2T_r} \tag{2.1.6}$$

where λ is the percent of superconductor, V is the conductor volume, and $2T_r$ is the ramp period for a complete monopolar cycle.

The SCDR proposed a 50 mm HEBDM using 2.5 μm conductor. An estimate of the heat generated during a monocycle for this magnet can be made assuming the following parameters: $d_f = 2.5\mu$m; $B_o = 1$ T; $J_c(B_o) = 10^{10} A/m^2$; $\lambda = 0.4$; $V = 0.0365 m^3$; $2T_r = 100s$; $B_2 = 7$ T; $B_1 = 2$ T. Using equation (2.1.6), we obtain the total power loss for both inner and outer conductors due to hysteresis in the superconductor, $\langle W_h^s \rangle = 5.2$ Watts for a magnet length of 15 m and a ramp time of 50 sec. from 0 to full field and ramp down at the same rate. The more accurate numerical solution using Morgan's J_c surface and an infinite-iron local magnetic fields gives 3.9 Watts for the same ramp cycle.

(2.2) Eddy currents in the strand

In twisted multifilamentary wires the superconducting filaments are coupled together by changing magnetic field. This coupling causes A.C. losses due to dB/dt related electric field rise along a zig-zag path as illustrated in figure (2.2a). The coupling losses are of an eddy current type. Thus the loss per cycle depends on the cycle ramp time, T_r.

To evaluate eddy current coupling losses in the HEBDM multifilamentary conductor strand, we use the anisotropic resistivity model[7]. This model assumes: 1) that the magnetic field within the composite is uniform, 2) the electric field lays entirely on the vertical

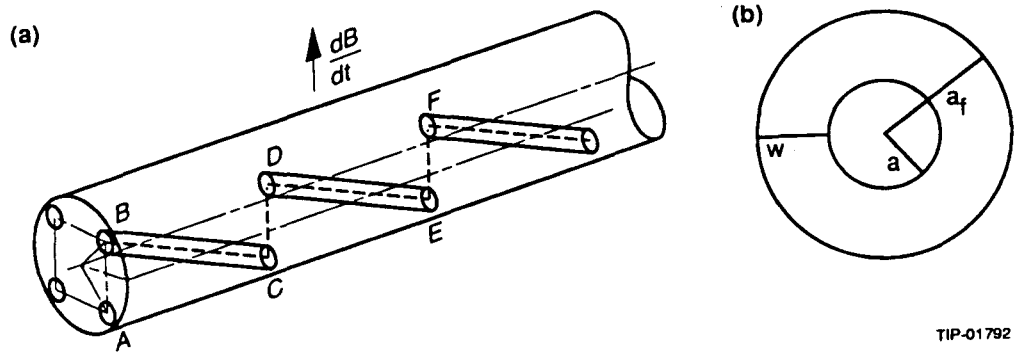

Figure 2.2 (a) - Filaments coupling model for multifilamentary superconductors and (b) - Strand cross-section used in effective transverse resistivity calculation.

part of the zig-zag path of the filament and the electric field along the electric center lines of the filaments and along the horizontal paths is zero, 3) only the filaments on the periphery of the composite are coupled and the interior filaments do not carry any coupling currents, 4) the transverse resistivity ρ_t across the composite lies between the two extreme resistivities: a) There is no contact resistance between filaments and the matrix transverse resistivity of the composite is:

$$\rho_t = \rho_m \frac{1-\lambda}{1+\lambda} \tag{2.2.1a}$$

where ρ_m is the matrix resistivity, and b) There is a high contact resistance between filaments and the matrix. The transverse resistivity is:

$$\rho_t = \rho_m \frac{1+\lambda}{1-\lambda}. \tag{2.2.1b}$$

The time decay is related to the effective resistivity and pitch length by the formula

$$\tau = \frac{\mu_o}{2\rho_{et}}\left(\frac{L}{2\pi}\right)^2. \tag{2.2.2}$$

This model gives the following formulae for the coupled eddy current power losses per unit volume:

$$\frac{W_e}{V} = \frac{\dot{B}_i^2}{\rho_{et}}\left(\frac{L}{2\pi}\right)^2 = \frac{2\dot{B}_i^2}{\mu_o}\tau \tag{2.2.3}$$

where $\dot{B}_i$ is the local time derivative of the magnetic field within the composite and τ can be estimated from strand magnetization data using the relationship:

$$2\dot{B}\tau = M_e.$$

Using strand data from A. Ghosh[8], with $M_e = 0.3$ mT for a conductor with a copper-to-superconductor ratio $\gamma = 1.5$ and a ramp rate of $\dot{B} = 0.021$, a $\tau = 7.1$ msec is obtained.

The second alternative involves estimating the effective transverse resistivity, ρ_{et}, of the eddy current path as

$$\rho_{et} = \frac{1}{\rho_t} + \frac{w}{a\rho_m} + \frac{aw}{\rho_m}\left(\frac{2\pi}{L}\right)^2$$

In figure (2.2b), a is the outer filament composite radius and ω is the thickness of the outer copper jacket. From equation (2.2.3), the resulting decay time is $\tau = 6.7$ msec. Data for 2.5 μm conductor is unavailable at the time of this report. It is difficult to predict the resistivity of the eddy current path. The 2.5 μm conductor is constructed such that the filaments are sub-bundled. Sub-bundles are separated by a copper matrix which could provide a low resistance path for eddy currents; however, some Cu-Ti compounds could be formed in the matrix which would increase the resistivity.

The eddy current power generated is

$$W_e = \int \tau \frac{2\dot{B}_i^2}{\mu_o} dV \tag{2.2.6}$$

where the integral is over the total conductor volume. Two solution techniques are used for the eddy current computation. Both are similar to the hysteresis calculations. In the analytic approximation, the average eddy current effect assuming a linear B field distribution in the coil volume ranging from B_1 to B_2. The resulting power generation expression is

$$\langle W_e \rangle^{st} = \frac{2V}{3\mu_o} \frac{B_2^3 - B_1^3}{B_2 - B_1} \frac{\tau}{T_r^2} \tag{2.2.7}$$

The analytic power expression yields a loss of 3.7 Watts assuming $B_1 = 2$ T and $B_2 = 7$ T. The numerical integration of equation (2.2.6) yields 3.4 Watts for the same $2T_r = 100$ seconds ramp cycle with a peak current of 6250 amperes (6.4T) for a 50 mm HEBDM. Scaling laws are used to represent the change in γ for the outer cable. A more complete table of losses has been included in section (2.6). The estimate of error in power loss from strand data is of the order of 30%.

(2.3) Eddy currents in the cable (strand-to-strand)

Strand-to-strand coupling in cabled conductors occurs when the single strands are not insulated and the contact resistance between them is low enough to achieve significant eddy current paths. The magnetic field induced currents pass across strand-to-strand interfaces causing eddy current type losses.

Evaluation of strand-to-strand losses presents challenging problems. Among the parameters which are unique to cabled superconductors are cable geometry and compaction (specifically during magnet fabrication) and strand interface conditions. Moreover during the magnet operation the cabled conductor experiences rather high electromagnetic forces which change the resistance between the strands. This resistance change is obviously a function of the magnetic induction, geometry of the coils, and the magnitude of pre-stress applied to the coil groups.

A few theoretical attempts have been made to evaluate analytically strand-to-strand coupling losses[9]. These models require strand-to-strand resistances or an effective decay time constant for the particular cable of given conditions emulating the coil conditions. These quantities must be experimentally determined. For instance, in the model proposed by Morgan[9] the strand-to-strand coupling losses for superconducting braids exposed to dipole field are given by the following expression:

$$W_e^{st} = \frac{N^2 h^2 L \dot{B}^2}{60R} \tag{2.3.1}$$

where W_e^{st} is in Watts per unit length of the braid, h is the width of the braid, L is the half braid pitch length, R is the crossover resistance of the braid, and N is the number of strands in the braid. The crossover resistance in the braid (or cable) is not directly measurable, since it is difficult to separate a single crossover or a few crossovers from the remainder of the braid. The resistance measurements and analysis which are required for determination of R are described by Morgan.[9] To evaluate interstand coupling losses for the 50 mm HEBDM conductor we have used the magnetization data obtained by A. Ghosh[8]. These data are based on comparison between the magnetization for a SSC cable with 23 strands stressed with 13

kpsi and the magnetization of the uncabled strands. The comparison shows that any excess magnetization due to interstrand coupling is $2M_e^{st} = 0.2 \pm 0.3$ mT. These measurements were carried out by comparing magnetization at ramp rates of 21 mT/sec and 42 mT/sec for cable samples.The rather high error in the measurements are related to experimental limitations. However analytical estimates like the ones showed above indicate that a value of 2 $M_e = 0.2$ mT is a reasonable estimate and the upper limit of 0.5 mT is too high. The time constant may be scaled using

$$\tau_{eff}^{st} = \tau_t(\frac{h}{h_t})^2 \frac{L}{L_t}(\frac{N}{N_t})^2 \tag{2.3.2}$$

where h_t is the test sample cable width, L_t is the test sample half pitch length, and N_t is the test sample number of strands. From this cable test $\tau_t = 2.4$ msec, $h_t = 0.0093$ m, $L_t = 0.0125$ m, and $N_t = 23$. The strand-to-strand eddy current power generated is

$$W_e^{st} = \int \tau^{st} \frac{2\dot{B}_i^2}{\mu_o} dV \tag{2.3.3}$$

which is an integral over all cable volume. The analytic field distribution approximation is

$$\langle W_e^{st} \rangle = \frac{2}{3\mu_o} V(1-\lambda) \frac{B_2^3 - B_1^3}{B_2 - B_1} \frac{\tau^{st}}{T_\tau^2} \tag{2.3.4}$$

The analytic model for the 50 mm HEBDM with 2.5 μm filament conductor has a $\tau_{eff}^{st} = 9.9$ msec and $\langle W_e^{st} \rangle = 3.4$ Watts.

The only significant τ_{eff}^{st} contribution is from B field component perpendicular to the cable width. The numerical simulation and numerical integrations with local B fields for (equation 2.3.3) and scale τ_{eff}^{st} by the B field orientation have been performed. The numerical result is obtained to be $W_e^{st} = 1.5$ Watts which is much lower than the analytic result due to the effect of field orientation, which was not taken into account in the analytical estimate.

(2.4) Proximity Effect Coupling Losses

The proximity effect can cause a time-independent interfilament coupling when the filament spacing is of the order of the superconducting coherence length. This coupling may produce rather high additional magnetization and hysteresis type losses in the superconductors with closely spaced fine filaments and low resistivity normal metal matrix. In some cases when the filament spacing is small but not enough to cause superconducting tunneling, the proximity effect can provoke a reduction of the transverse resistivity and unacceptable enhancement of the standard coupling between the filaments.

In any case, to reduce or avoid proximity effect losses the filament spacing should be increased or some impurities must be introduced to the matrix. The impurities, typically Ni or Mn, increase the electron scattering and therefore reduce the superconducting coherence length in the matrix material. As a result, proximity effect coupling vanishes. However, increased matrix resistance could effect the conductor stability and quench performance if the copper core or jacket are affected by the impurities.

To evaluate the proximity effect losses for 2.5 μm filament HEBDM cable, we adopt the model proposed by M. Green[10]. This model gives the magnetization due to proximity effect coupling as:

$$M_{prox} = \frac{2}{3\pi\mu_o} \frac{d_s J_c}{\gamma + 1} e^{-\epsilon} \tag{2.4.1}$$

where d_s is the strand diameter, γ is the copper to superconductor ratio, and

$$\epsilon = 7.18 \times 10^{11}(B + 0.5)[W\sqrt{\rho_t} - 7.8 \times 10^{-12}] \tag{2.4.2}$$

and $\rho_t = 6.56 \times 10^{-6}/W + \rho_m$.

Table 2.5 Yoke Hysteresis Effects				
Material	Coercivity	Q/V	Q/V/Oe	W/V*
A-36	3.1 Oe	1950 J/M^3	630	9.8
Kawasaki	1.25 Oe	763 J/M^3	610	3.8
Armco	0.6 Oe	336 J/M^3	560	1.7
$\star$ evaluated at $T_r = 50$				

It appears that equation (2.4.1) cannot predict the onset of proximity coupling very well. For instance, the proximity coupling magnetization of 2.5 μm filament with Cu matrix conductor and filament spacing of 0.33 μm at $B = 0$ is rather high. Equation (2.4.1) predicts a value of $M_{prox} = 52$ mT. In our opinion, the filament spacing of 0.33 μm in a copper matrix with possible Cu-Ti compound formation is effective enough to prevent proximity coupling because the coherence length in the Cu 'dirty' limit with $l_n \cong 10^{-8}$m at 4.2K is $\xi \cong 340\mathring{A}$ i.e. one order of magnitude smaller than the filament spacing.[6]

In the case of Cu-Mn with 0.5 wt. % Mn, M_{prox} is very small because $\rho_m = 2.11 \times 10^{-8}\Omega$m for this alloy at 4.2K.[11] As we have already mentioned, the possible change of stability, however, has to be considered if the Cu-Mn alloy will be used as the matrix material.

In conclusion, we must point out that in principle two other sources of loss could exist: penetration loss which can occur due to the induced coupling currents driving the outermost filaments of the composite into the critical state and cause additional hysteresis type losses, and additional loss can also occur during to self-field influence on the transport current distribution within the conductor. We have neglected these losses in our estimates.

(2.5) Yoke hysteresis

Another significant source of heat generation is the magnetization in ferromagnetic materials. Superconducting accelerator magnets use low carbon steel usually having a coercivity of 0.8 to 3.0 Oersted. If the material properties are well known, it is relatively easy to compute the heat generated by integrating the area inside the hysteresis loop:

$$Q = \int_{vol} \int_{cycle} M dB dV \tag{2.5.1}$$

The saturation magnetization point is approximately 1.6 T–2.1 T where the loop closes. A small but significant percentage of the iron in a dipole magnet does not reach 1.6 T and therefore forming a smaller hysteresis loop. Finite element saturable iron calculations reveal that between 60- 80% of the yoke is saturated to beyond 1.6 T depending on the design and peak field operating conditions. A weighted contributed volume, V^*, can be estimated from F.E. models of yoke saturation

$$W_y = \frac{V^*}{T_r} \int_0^{B_{max}} M dB \tag{2.5.2}$$

Results are very dependent on material properties. Since the low temperature coercivity is not currently known, the actual A.C. loss due to yoke hysteresis could be higher than the estimates in this paper. However, measurements on a limited number of materials both at 300K and 4.2K suggest that there is little change in coercivity.[12]

The area inside the magnetization loop scales linearly with the coercivity as seen in table (2.5). Data indicates that the hysteresis area scales as $B^{1.6}$ where B is the peak field seen by the iron. Once low temperature data is available for selected materials, corrections of estimates can be made using this scaling information.

In conclusion, yoke hysteresis losses scale linearly with the coercivity yielding approximately 600 joules per meter^3-Oersted. Little data is available for temperatures near 4K and these models use room temperature magnetization data. Clearly, more information is needed for cryogenic temperatures.

It must be pointed out that the yoke hysteresis loss estimated above is applicable only to a bipolar (truly AC) operation. If the magnet were to be operated as a monopolar device, the yoke loss is expected to reduce significantly.

(2.6) Summary of A.C. losses

Table (2.6) provides a summary of power loads for varying magnet designs. These results are based on a ramp time of $T_r = 50$ sec. without rest period. All hysteresis effects and allowances for rest periods scale as

$$W_h = W_h^{(50)}(\frac{50}{T_r}).$$

The results in this paper represent the impact of a full hysteresis loop. If the area inside the yoke iron hysteresis loop is small for a monopolar operation compared to the bipolar operation this would make a significant impact on cryogenic needs. All eddy current effects are dB/dt dependent and scale as

$$W_e = W_e^{(50)}(\frac{50}{T_r})^2.$$

The time dependence of eddy current losses implies that significant heat load reduction would accompany slower ramp rates.

Table 2.6 Summary of A.C. Losses

	CDM 50 mm		HEB 60 mm T5		HEB 60 mm T11	
	2.5 μm	6.0 μm	2.5 μm	6.0 μm	2.5 μm	6.0 μm
1.8Tev (5.8T)						
amps	5650	5650	5950	5950		
Cable Hys.	3.9	9.3	3.9	9.3		
strand eddy	2.6	2.6	2.7	2.7		
cable eddy	1.2	1.2	0.9	0.9		
yoke Hys.	2.4	2.4	2.4	2.4		
Total Watts						
Case 1	10.1	15.5	9.9	15.3		
Case 2	8.4	12.9	8.2	12.7		
Case 3	3.7	6.2	3.7	6.1		
2.0Tev (6.38T)					1.96 TeV	(6.25T)
amps	6250	6250	6600	6600	6500	6500
Cable Hys.	3.9	9.3	3.9	9.3	5.3	12.7
strand eddy	3.2	3.2	3.3	3.3	4.2	4.2
cable eddy	1.5	1.5	1.0	1.0	3.2	3.2
yoke Hys.	3.1	3.1	3.1	3.1	3.8	3.8
Total Watts						
Case 1	11.7	17.1	11.3	16.7	16.4	23.9
Case 2	9.8	14.3	9.4	13.9	13.7	19.9
Case 3	4.3	6.7	4.2	6.6	5.8	9.2

Case 1 $T_r = 50$ with no rest period
Case 2 $T_r = 50$ with 10 sec rest period
Case 3 $T_r = 100$ with 10 sec rest period

The comparisons in table (2.6) for the T5 design and the CDM designs are listed for two injection energies. If the injection energy is 2 TeV for both magnets with 6 μm filament conductor, the total A.C. loss for the T5 design is 15.3 Watts and for the CDM design is 15.5 Watts. With equivalent operational parameters, these two designs produce approximately the same power.

Cases 2 and 3 represent realistic ramp cycles with rest periods. Case 2 represents the 'peak' performance of the HEB ring and case 3 is the specification required in the SCDR. With regards to acceptable cryogenic performance for a given lattice, three parameters can be tuned: 1) ramp cycle rate, 2) injection energy, and 3) choice of monopolar vs bipolar cycles. As seen in figure (2.6) the ramp rate has a large heat load impact. The impact of monopolar vs. bipolar cycling would need to be determined experimentally. There is little impact in changing the injection energy from 2.0TeV to 1.8TeV.

The T5 60 mm HEBDM design is approximately 10–20% more efficient than the 50 mm CDM design due to the reduction of peak current (and field) , less yoke volume, and less yoke saturation. The CDM and T5 designs have an approximate saturation of 85% at 6.38T and 60% at 5.8T. The T11 60 mm design has a much larger heat load associated with a larger volume of superconductor and of yoke.

Assuming no impact from proximity effects and that eddy current contributions do not vary drastically between 6 μm and 2.5 μm filament conductor, there is a significant difference between the heat loads of these two filament types. The manufacturability of 2.5 μm filament conductor may be a design consideration but, this issue is beyond the scope of this report.

(3) DISCUSSION AND CONCLUSIONS

The T5 and T11 designs conclusions are based on yoke geometries which do not include keys, bus bar, helium bypass holes, and other features. A real magnet will exhibit additional saturation effects and modified hysteresis effects due to these features. As discussed previously, the major sources of cryogenic heat load are from hysteresis in the superconductor, hysteresis in the yoke, and eddy currents in the cable. There are a number of uncertainties in determination of A.C. losses of real superconducting magnets. In magnet conductors or cables the critical current density can vary with their length due to non-ideal geometry and source technology factors: sausaging, local stress, nonuniformity of cabling, etc. A.C. losses could be also affected by self-welded, touched, or sub-bundled filaments, or by local differences in matrix resistivity due to different deformation history an incomplete final anealing, or by Cu-Ti formation. As previously discussed, interstrand losses strongly depend on compaction and surface conditions of the wires which can also differ with their length.

Hysteresis losses in the magnet yoke can not be calculated precisely at present due to a lack of information for the properties of low carbon steel near 4.2K. In addition, the precise determination in a magnet may require knowledge of magnetization stress dependence at low temperatures. However, recent manufacturing techniques (e.g. in Armco) have provided low coercivity iron (0.6 oe) and use of this is contemplated for the HEB after qualification and testing and this could render the yoke loss unimportant.

The models for A.C. loss determination discussed above assume approximations which can have significant effect. For instance A.C. loss evaluation in the vicinity of H_{c1} is rather simplified. Since the critical state model enables the determination of $\nabla \times \vec{B}$ but not $\nabla \times \vec{H}$ (the free current density which is necessary for a loss calculation) it is assumed that $H = B/\mu_o$ which is a very rough approximation for the region near zero field. As known the reversible magnetization curve for hard type II superconductors can not be theoretically determined or experimentally obtained.

The estimated error for the total A.C. losses is on the order of 30%. Very preliminary experimental results are larger than this estimated loss by 50-100%.[13] More experiments must be performed to resolve the A.C. losses heat load for HEB design considerations.

Finally, a significant source of energy loss could arise from purely mechanical causes. It is known that the magnet coils have a hysteretic stress-strain curve and the cycling of the coil stresses during ramp cycles could result in the release of frictional energies stored in the

stress-strain hysteresis. This effect is known to be very strongly dependent upon details of the magnet, preconditioning and thermal cycling. This analysis has not attempted to include this effect.

The above sources of error and uncertainties will be addressed through a program of experimental measurements and tests. These include a more accurate measurement of strand eddy current magnetization, strand to strand coupling effects using wider and larger number of strands or by using higher ramp rate, and measurement of iron magnetization at low temperatures . A comprehensive A.C. loss testing program is under way to measure the loss in 50 mm model magnets and this will be supplemented by a long magnet test in future.

A modification of the T5 60 mm HEBDM design would provide an acceptable design for the HEB lattice provided that 1.8 TeV is the collider injection energy. The A.C. losses generated by this magnet will range from 10 to 15 Watts per fifteen meter magnet assuming that $2T_r = 100$ seconds. The 2.5 μm filament conductor is still an appealing option to reduce A.C. losses although it may be possible to use 6 μm filament conductor.

References

1. D. Johnson, private communication.

2. J.R. Sanford and D.M. Matthews, ed., internal report SSCL-SR-1056 (1990).

3. B. Aksel, private communication.

4. D. Orrell, private communication.

5. G. Morgan, private communication.

6. V. Kovachev, **Energy Dissipation in Superconducting Materials**, Clarendon Press, Oxford, UK, 1991.

7. M. Wilson, **Superconducting Magnets**, Clarendon Press, Oxford, UK, 1983.

8. A.K. Ghosh, private communication.

9. G. Morgan, J. Appl. Phys., 44, 3319 (1973).

10. M. Green, Adv. Cryo. Eng. **33**, 149 (1987).

11. N. Sadakata, M. Sugimoto, M. Tange, O. Kohno, Proc. MT-11, Tsukuba, Japan, **2**, 944 (1989).

12. A.K. Ghosh and K.E. Robins, "Magnetization Measurement of Low Carbon Steel", Technical Note No. 371, Brookhaven National Laboratory (1982).

13. Unpublished preliminary results from Fermi National Accelerator Laboratory.